J Mater Sci (2007) 42:1955–1964
DOI 10.1007/s10853-006-0452-6

NONSTOICHIOMETRIC COMPOUNDS

Stability and defect structure of spinels $Li_{1+x}Mn_{2-x}O_{4-\delta}$: I. In situ investigations on the stability field of the spinel phase

Chunhui Luo · Manfred Martin

Received: 19 March 2006 / Accepted: 11 May 2006 Published online: 13 January 2007

Abstract The stability field of the Li–Mn–O spinel, $Li_{1+x}Mn_{2-x}O_{4-\delta}$, was investigated as a function of temperature, T, cation composition, n_{Li}/n_{Mn}, and oxygen partial pressure, pO_2, by means of in situ X-ray diffraction (XRD) and thermogravimetry (TG). In a T-n_{Li}/n_{Mn} phase diagram, the stability field is described by the upper and lower critical temperatures, T_{c1} and T_{cL}, respectively. Above T_{c1}, Li_2MnO_3 is formed as a second phase, and below T_{cL} Mn_2O_3 is formed. Both T_{c1} and T_{cL} decrease continuously with increasing n_{Li}/n_{Mn} and increase with increasing pO_2. The single phase region contains lithium-deficient and lithium-excess spinels, and no discontinuous change of the critical temperature curves was found at $n_{Li}/n_{Mn} = 0.5$, corresponding to $LiMn_2O_4$. With the experimental data obtained in this work, a three-dimensional stability field of the Li–Mn–O spinel phase diagram is put forward to describe the relationship between T, n_{Li}/n_{Mn} and pO_2. In addition, the upper critical temperature, T_{c1}, was investigated for spinels doped with Ni, Co and Mg. For all three dopants, T_{c1} decreases with increasing dopant concentration.

Introduction

Lithium manganese oxide spinel has been studied extensively as a potential cathode material for rechargeable lithium ion batteries, due to its low cost, limited environmental impact and excellent voltage characteristics compared to traditional materials such as $LiCoO_2$ [1–4]. The lattice symmetry of the spinel $Li[Mn_2]O_4$ is cubic (space group *Fd3m*) with a lattice constant of about 824.8 pm [5, 6]. The oxygen ions, located in the 32*e* sites, form a cubic-close-packed array, where only one-eighth of the 64 tetrahedral sites is occupied by lithium ions (8*a*) and one-half of the 32 octahedral sites by manganese ions [16*d*]. In this structure, it is easy to accommodate small guest ions, such as excess lithium ions, on interstitial positions. However, $Li[Mn_2]O_4$ shows significant capacity fading and poor cycle ability, when it is cycled in the 3–4 V voltage range. To explain the poor cycling performance, where the crystal symmetry was reduced from cubic to tetragonal [7, 8], a Jahn–Teller distortion was proposed. It is commonly believed that the Jahn–Teller distortion results from the instability of trivalent manganese ions in the octahedral sites. In recent years many researchers concentrated on solving this problem, in principle, by decreasing the Mn^{3+} ion concentration, or in other words, increasing the average valence of manganese. Two basic methods were applied: (1) replacing a small amount of manganese by excess monovalent Li or doping with di- or trivalent metals (Mg, Ca, Zn, Co, Al, Cr, etc.) [9–18]; (2) introducing defects such as cation and oxygen vacancies or cation interstitials into the spinel structure by synthesizing the spinel at higher oxygen partial pressures, pO_2 [19–22].

The Li-doped (or Li-excess) spinel has a regular formula $Li_{tet}[Li_xMn_{2-x}]_{oct}O_{4-\delta}$ ($0 \le x \le 0.33$), where the excess lithium ions replace manganese ions on the octahedral sites [23] and δ refers to the oxygen

C. Luo · M. Martin (✉)
Institute of Physical Chemistry, RWTH Aachen University, Landoltweg 2, Aachen 52056, Germany
e-mail: martin@rwth-aachen.de

nonstoichiometry. According to the phase diagram of the Li–Mn–O system in air between 350 and 1060 °C determined by Paulsen and Dahn [24] single phase lithium-excess spinels, $Li_{1+x}Mn_{2-x}O_4$ ($0 \le x \le 0.33$), are stable between 400 and 880 °C (with an average Mn valence between 3.5 and 4). The single phase cubic spinel region is constricted between two critical temperatures. Above the upper critical temperature line, T_{c1}, the spinel coexists with monoclinic Li_2MnO_3 [25–28] and below the lower critical temperature line, T_{cL}, with Mn_2O_3 or MnO_2 [27, 29], respectively. T_{c1} has been investigated as a function of lithium content, x [26, 30–32], and oxygen partial pressure, pO_2 [33]. However, to our knowledge the lower critical temperature, T_{cL}, has not been exactly determined until now, probably because of the slow kinetics at lower temperature and the small Mn_2O_3 concentration, resulting in long equilibration times and low-level X-ray diffraction intensities [30]. Above the critical temperature $T_{c2} \approx 940$ °C the new phase $LiMnO_2$ starts to form [24].

In the lithium deficient spinel, it is generally considered that the excess Mn ions substitute Li ions in tetrahedral 8*a* sites as Mn^{2+}, which is described by the formula $\left(Li_{1-x}Mn_x^{2+}\right)_{tet}\left[Mn_{1-x}^{4+}Mn_{1+x}^{3+}\right]_{oct}O_4$ [34]. For charge compensation, a corresponding proportion of Mn^{4+} ions on octahedral 16*d* sites are reduced to Mn^{3+}. However, the increase of the Mn^{3+} concentration could result in the occurrence of a Jahn–Teller distortion, and the structure becomes tetragonal (space group *I41/amd*).

In a previous article [35] we have reported on our preliminary results of in situ investigations of the stability field of the Li–Mn–O spinel by means of X-ray diffraction (XRD) and thermogravimetry (TG) and also on the first results of thermogravimetric experiments on the defect structure of the spinel. In this article (part I), we report comprehensive experiments on the stability conditions of Li–Mn–O spinel with Li-excess and Li-deficit and also of spinels doped with Ni, Co and Mg. The stability field of single phase spinel was determined as a function of temperature, T, cation composition, n_{Li}/n_{Mn}, oxygen partial pressure, pO_2, and dopant concentration by in situ XRD and TG. Our results on the spinel stability field form the basis for investigations on the high temperature defect structure of lithium–manganese spinel that will be published in a forthcoming article (part II, [36]). From the measured mass changes after isothermal pO_2-jumps the nonstoichiometry, δ, of the spinel $Li_{1+x}Mn_{2-x}O_{4-\delta}$ can be obtained and will be modeled in terms of possible defects in the cation, anion and interstitial sublattices.

Schematic spinel stability field and experimental strategy

Before we report on the experimental techniques and results we will discuss shortly the schematic stability field of the Li–Mn–O spinel to describe our experimental approach during the in situ XRD and TG experiments. In the ternary system Li–Mn–O there are four independent thermodynamic variables: total pressure, p, temperature, T, oxygen partial pressure, pO_2, and cation composition. Concerning the cation composition, only the ratio $r = n_{Li}/n_{Mn}$ can be fixed experimentally (see also Section ''Experimental''), where n_{Li} and n_{Mn} are the molar quantities of Li and Mn. Normalizing the sum of the cation fractions to 3, the spinel can be written as $Li_{1+x}Mn_{2-x}O_{4-\delta}$, where x is given by $(2r-1)/(1+r)$. A ratio $r = 1/2$ corresponds to $x = 0$, $r > 1/2$ to Li-excess ($x > 0$) and $r < 1/2$ to Li-deficit ($x < 0$), and all possible defects (e.g. cation vacancies, cation interstitials, oxygen vacancies ...) are summarized in the nonstoichiometry δ (that depends again on p, T, pO_2 and n_{Li}/n_{Mn}). In Fig. 1 a schematic stability field of the Li–Mn–O spinel is shown in a plot temperature, T, versus cation composition, $r = n_{Li}/n_{Mn}$, for constant total pressure, p, and constant oxygen partial pressure, pO_2.

The single phase Li–Mn–O spinel (region I) exists only below the upper critical temperature curve, $T_{c1}(r)$, and above the lower critical temperature curve, $T_{cL}(r)$, while in region II the spinel coexists with Li_2MnO_3 and in region III with Mn_2O_3.

The three different regions can be identified by means of in situ X-ray diffraction experiments by the appearance of the diffraction patterns of the corresponding phases. However, near the critical temperature curves separating the single phase region from a

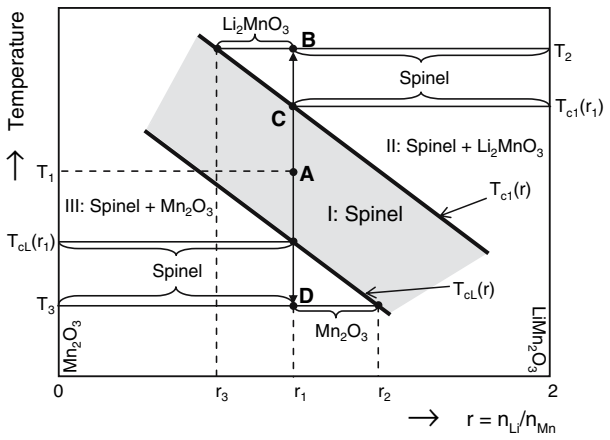

Fig. 1 Schematic stability field of the Li–Mn–O spinel and decomposition during heating and cooling

two phase regions, the amount of Mn_2O_3 or of Li_2MnO_3 becomes very small and these phases are hard to detect by XRD. Thus these measurements will only allow for a rough determination of the transition temperatures.

A more accurate determination of the transition temperatures is possible by thermogravimetry (TG). If a spinel sample of defined composition, r_1, is first equilibrated at temperature T_1 (point A within region I, as identified by in situ XRD) and then heated to temperature T_2 in region II (point B) the following reaction takes place:

$$a_1 \cdot Li_{1+x1}Mn_{2-x1}O_{4-\delta1} \xrightarrow{\text{Heating}} a_2 \cdot Li_{1+x2}Mn_{2-x2}O_{4-\delta2} + b_2 \cdot Li_2MnO_3 + c_2 \cdot O_2(g) \quad (1)$$

During heating, but still within the stability field of the spinel, i.e. for $T < T_{c1}(r_1)$, we have $a_1 = a_2$ and $b_2 = 0$. Thus the amount of reacted oxygen, c_2, is only due to a change of the nonstoichiometry of the spinel, $c_2 = ½ \cdot a_1 \cdot (\delta_2\text{-}\delta_1)$, and we expect only a very small mass change during a TG-experiment. If, however, the temperature rises above the critical temperature, $T_{c1}(r_1)$, the spinel decomposes into a spinel with lower Li-content and Li_2MnO_3, resulting in a much larger mass change during the course of the reaction. Thus, the discontinuous change in the slope of the TG-signal renders possible the accurate determination of the transition temperature, $T_{c1}(r_1)$. By repeating this procedure for several initial spinel compositions the curve $T_{cL}(r)$ can be obtained.

If, on the other hand, a single point on the curve of the upper critical temperature is known, e.g. point C in Fig. 1, this point can be taken as a reference point. Heating the single phase spinel from $T_{c1}(r_1)$ to T_2, the amounts of spinel, $a_2(T)$, and of Li_2MnO_3, $b_2(T)$, as well as the cation composition, $x_2(T)$, can be determined by measuring the mass change, $c_2(T)$, during heating and using the three mass balances for Li, Mn and O. Here we neglect the nonstoichiometry, δ, in Eq. (1), assuming that it is small compared to the amount of reacted oxygen, c_2. In this way, the whole curve, $T_{c1}(r)$, can be obtained for $T > T_{c1}(r_1)$ from a single TG-experiment. The applicability of this method requires, however, a fast kinetics for the reaction in Eq. (1) or a slow heating rate during the TG experiments.

Cooling a single phase spinel at point A in region I to point D in region III, the spinel first changes its stoichiometry ($T > T_{cL}(r_1)$), and, starting at $T_{cL}(r_1)$, then decomposes into a spinel with higher Li-content and Mn_2O_3.

$$a_1 \cdot Li_{1+x1}Mn_{2-x1}O_{4-\delta1} \xrightarrow{\text{Cooling}} a_3 \cdot Li_{1+x3}Mn_{2-x3}O_{4-\delta3} + b_3 \cdot Mn_2O_3 + c_3 \cdot O_2(g) \quad (2)$$

Thus, the lower critical temperature, $T_{cL}(r_1)$, can be determined in the same way as described above for $T_{c1}(r_1)$, i.e. from the discontinuous change of the slope of the TG-signal.

Experimental

A series of Li–Mn–O and Li–Mn–Me–O (Me = Mg, Ni, Co) spinel samples were prepared by the modified Pechini method [37–41] that has many advantages compared to the conventional solid-state reaction method: good stoichiometry control, fine particles with narrow particle-size distribution, shorter processing times and lower calcination temperatures. The preparation starts with solutions of lithium nitrate and manganese nitrate of the proper molar ratio. Citric acid and ethylene glycol with a molar ratio of 1:4 were used as the joint emulsion. After evaporation under continuous stirring at 90 °C and self-combustion, the homogeneous solution turns into a fine black precursor. The precursor was sintered in air, firstly at 350 °C for 48 h, then at 750 °C for 4 h, and finally cooled down to room temperature at a rate of 5 °C/min. The cation composition of these as-prepared samples was analyzed by means of Inductively Coupled Plasma with Optical Emission Spectroscopy (ICP-OES). Prior to all further measurements, X-ray diffraction patterns (Stadi P, Stoe&Cie) were taken at room temperature to check whether all samples are single phase Li–Mn–O spinels. Either copper (Cu K_α, $\lambda = 154.056$ pm) or cobalt (Co K_α, $\lambda = 178.9007$ pm) radiation was used.

In order to determine the stability field of the spinel at elevated temperatures the samples were investigated by in situ XRD on a theta–theta X-ray powder diffractometer (Stoe&Cie) using copper radiation. The diffractometer is equipped with a heating chamber (Buehler HDK 2.4 a). The measurements were performed at $pO_2 = 0.2$ bar, and the as-prepared samples were firstly heated at a rate of 10 °C/min to 1000 °C. After holding the temperature for 1 h an in situ diffractogram was taken (acquisition time 1 h). The samples were then cooled down with a rate of 10 °C/min. Every 50 °C the temperature was first held for an hour and then an in situ diffractogram was taken (acquisition time 1 h between 1000 and 550 °C and 2 h between 500 and 300 °C).

Thermogravimetry measurements (TG) were performed on a thermobalance (Setaram Setsys 16/18), that has a maximum sensitivity of 0.04 μg. The TG curves were recorded starting with the as-prepared samples during sample heating/cooling between room temperature and 1000 °C at a constant rate of 1 °C/min under well-defined oxygen partial pressures, pO_2. The required oxygen partial pressure was established by mixing nitrogen and oxygen and controlling the flow rates of both gases.

Results and discussion

Chemical analysis

The composition of the as-prepared samples as determined by ICP-OES analysis is shown in Tables 1 and 2. It is found that all samples possess a slightly smaller lithium content than initially weighted in. A similar lithium loss was also reported in literature and explained by lithium evaporating during the synthesis due to the high temperature during the self ignition process [41].

In situ XRD

At first results obtained for a lithium excess spinel ($n_{Li}/n_{Mn} = 0.564$) will be discussed. Its lattice parameter calculated from the XRD pattern at room temperature is 821.8 pm and smaller than that of the spinel $LiMn_2O_4$ ($a = 824.762$ pm). This finding agrees with earlier reports [42, 43] on a decrease of the lattice constant with increasing lithium content in the spinel phase (and is caused by the fact that the Li-excess is compensated by an increasing amount of Mn^{4+} with a smaller ionic radius than Mn^{3+}).

Table 1 Cation composition of as-prepared Li–Mn–O spinels as determined by ICP-OES

Li–Mn–O sample	Li (wt.%)	Mn (wt.%)	n_{Li}/n_{Mn}
LMO-1	3.36 ± 0.08	58.4 ± 0.5	0.455
LMO-2	3.57 ± 0.07	59.2 ± 0.4	0.477
LMO-3	3.64 ± 0.05	59.4 ± 0.5	0.485
LMO-4	3.8 ± 0.05	61.0 ± 0.4	0.493
LMO-5	3.9 ± 0.08	60.5 ± 0.7	0.510
LMO-6	4.16 ± 0.05	58.9 ± 0.7	0.559
LMO-7	4.18 ± 0.06	58.7 ± 0.3	0.564
LMO-8	4.2 ± 0.2	56.4 ± 0.4	0.589
LMO-9	4.58 ± 0.07	58.1 ± 0.6	0.624
LMO-10	4.8 ± 0.2	55.4 ± 0.5	0.686
LMO-11	5.33 ± 0.08	55.9 ± 0.9	0.755

Table 2 Cation composition of Li–Mn–Me–O spinels (Me = Mg, Ni, Co) as determined by ICP-OES

Li–Mn–Me–O sample	Li (wt.%)	Me (wt.%)	Mn (wt.%)	$n_{Li}/(n_{Mn} + n_{Me})$	$n_{Me}/(n_{Mn} + n_{Me})$
Mg-1	3.71 ± 0.07	0.66 ± 0.02	58.6 ± 0.5	0.489	0.025
Mg-2	3.74 ± 0.06	1.31 ± 0.02	57.0 ± 0.3	0.494	0.049
Mg-3	3.67 ± 0.06	1.98 ± 0.03	55.6 ± 0.4	0.484	0.074
Mg-4	3.74 ± 0.08	2.70 ± 0.03	55.8 ± 0.2	0.478	0.099
Ni-1	3.6 ± 0.07	1.6 ± 0.09	58.1 ± 0.3	0.478	0.025
Ni-2	3.6 ± 0.06	3.1 ± 0.05	56.0 ± 0.5	0.484	0.049
Ni-3	3.6 ± 0.06	4.8 ± 0.07	55.4 ± 0.4	0.476	0.075
Ni-4	3.7 ± 0.06	6.6 ± 0.2	53.3 ± 0.4	0.492	0.104
Co-1	3.7 ± 0.1	1.7 ± 0.02	57.0 ± 0.5	0.500	0.027
Co-2	3.6 ± 0.08	3.4 ± 0.07	56.9 ± 0.5	0.474	0.053
Co-3	3.7 ± 0.08	5.1 ± 0.09	55.6 ± 0.9	0.485	0.079
Co-4	3.7 ± 0.07	6.8 ± 0.1	54.9 ± 0.9	0.478	0.103

Figure 2 shows a series of in situ XRD powder patterns of the lithium excess sample ($n_{Li}/n_{Mn} = 0.564$) that were collected during cooling from 1000 °C under $pO_2 = 0.2$ bar. At temperatures above 700 °C, two phases are found, $LiMn_2O_4$ (JCPDS 27-1252) and Li_2MnO_3 (JCPDS 35-0782). With decreasing temperature, the intensities of the Li_2MnO_3 peaks decrease, while those of the spinel peaks increase. Below 650 °C only single phase spinel peaks were detected.[1] These findings give direct evidence of the decomposition of the spinel phase at higher temperatures via Eq. (1). Thus, according to in situ XRD analysis, the upper critical temperature of the single phase spinel region, T_{c1}, lies between 650 and 700 °C for a spinel with a cation composition $n_{Li}/n_{Mn} = 0.564$.

In the same way, the in situ XRD patterns for a sample with lithium deficit ($n_{Li}/n_{Mn} = 0.455$) were collected during cooling from 1000 °C at $pO_2 = 0.2$ bar (see Fig. 3). It can be seen that at temperatures above 900 °C the sample with lithium deficit exhibits the same behavior as that with lithium excess, i.e. the single phase spinel decomposes into a two-phase mixture containing spinel and Li_2MnO_3, and the intensities of the spinel phase increase and those of Li_2MnO_3 decrease during cooling, respectively. However, the critical temperature of the decomposition (between 850 and 900 °C) is higher than that of the Li excess spinel, which indicates a better stability of the lithium deficient spinel. At room temperature peaks of the second phase Mn_2O_3 (JCPDS 89-4836) were also

[1] The shift of the peaks in Fig. 2 between room temperature and higher temperatures is caused by thermal expansion of the sample and—to a larger extend—by thermal expansion of the heating element resulting in a slight misalignment of the sample in the X-ray diffractometer.

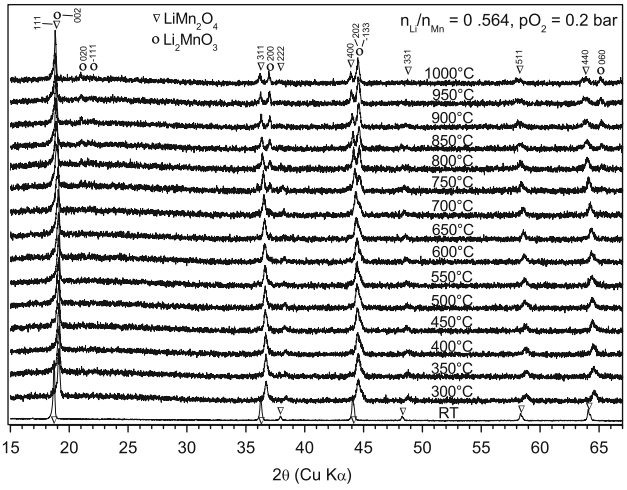

Fig. 2 In situ XRD patterns during cooling of Li-excess spinel ($n_{Li}/n_{Mn} = 0.564$): ∇ = $LiMn_2O_4$ (35-0782), ○ = Li_2MnO_3 (27-1252)

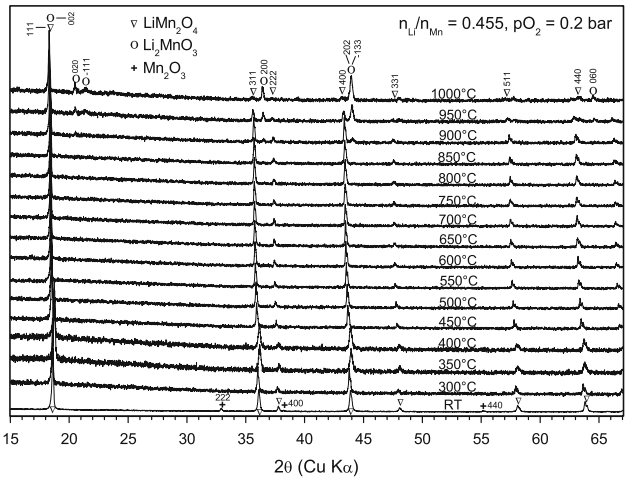

Fig. 3 In situ XRD patterns during cooling of Li-deficient spinel ($n_{Li}/n_{Mn} = 0.455$): ∇ = $LiMn_2O_4$ (35-0782), ○ = Li_2MnO_3 (27-1252), + = Mn_2O_3 (89-4836)

found. They could not be detected in the diffractograms taken at higher temperatures. This is probably due to the noise in the in situ diffractograms and the slow kinetics at low temperatures resulting in small intensities of the Mn_2O_3 peaks.

The temperature intervals for the upper critical temperature, T_{c1}, that were obtained by in situ XRD are shown in Table 3. The upper critical temperature, T_{c1}, where Li_2MnO_3 disappears during cooling, decreases with increasing n_{Li}/n_{Mn}. As peaks of Mn_2O_3 were detected only for samples with strong lithium deficit at room temperature, the transformation temperature between the two-phase mixture (Mn_2O_3 and spinel) and the single phase spinel, T_{cL}, is difficult to determine by in situ XRD as already mentioned in Paulsen's work [24]. Moreover, the [220] peak at $2\theta = 30.7°$, which indicates Mn on tetrahedral sites of the lithium deficient spinel [24, 44] was not found in our measurements of lithium deficient spinels. Single phase spinel without Mn on the tetrahedral sites for even lower Li-content was also confirmed by Xia et al. [45]. It seems that our air-prepared spinel with $n_{Li}/n_{Mn} < 0.5$ has—even at elevated temperatures—a manganese distribution, which is different from that reported by Björk et al. [46] and Paulsen and Dahn [24].

Table 3 Upper critical temperature, T_{c1}, as determined by in situ X-ray diffraction in air

n_{Li}/n_{Mn}	0.455	0.510	0.564
T_{c1} (°C)	850–900	750–800	650–700

The splitting of the [311] peak of the cubic $LiMn_2O_4$ spinel into the [311] and [113] peaks of the tetragonally distorted spinel, which would be an indication of a Jahn–Teller distortion, was not found in our in situ XRD patterns. It must be emphasized, however, that the tetragonal spinel reported by Yamada et al. [33] and Tarascon et al. [34] was found by them in quenched samples and only in a small temperature interval (about 900–950 °C), where both Li_2MnO_3 and $LiMnO_2$ disappear according to their XRD patterns. According to our findings based on in situ experiments, at these temperatures the cubic spinel coexists always with Li_2MnO_3, as found also by Thackeray et al. [26]. It implies that the formation of tetragonal spinel reported in [33, 34] resulted probably from the quenching process.

Thermogravimetry

A typical TG plot collected for a sample with Li-excess, $n_{Li}/n_{Mn} = 0.564$, is shown in Fig. 4. The sample was heated from room temperature up to 1000 °C at 1 °C/min under $pO_2 = 0.2$ bar. As water was already desorbed at lower temperatures, the initial weight loss could result from the loss of oxygen according to Eq. (1) and/or Li_2O evaporation, where the latter process is not reversible. No evident irreversible weight loss was found after heating and cooling cycles in the temperature region of our measurements. It was also reported by Paulsen et al. and Thackeray et al. [24, 26] that Li_2O evaporates only at temperatures above 1200 °C. Thus, the effect of Li_2O evaporation will not be discussed further in this article.

As described in Section ''Schematic spinel stability field and experimental strategy'' a discontinuous change in the slope of the TG signal is expected if

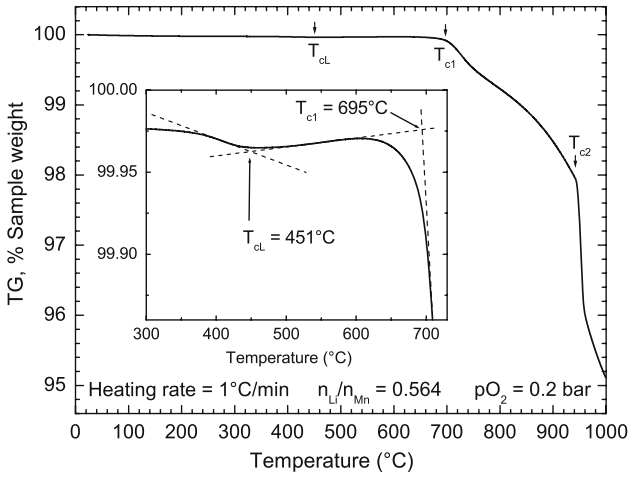

Fig. 4 Relative mass change during heating of a Li-excess spinel (n_{Li}/n_{Mn} = 0.564) from RT to 1000 °C. The inset displays how the critical temperatures, T_{cL} and T_{c1}, were determined. At T_{c2} $LiMnO_2$ starts to form

the boundary of the spinel stability field is crossed during cooling or heating (see Eqs. (1) and (2)). The first discontinuous change of the slope in the TG plot in Fig. 4 appears at 451 ± 3 °C.[2] Thus we assume that this temperature is the lower critical temperature, T_{cL} (see Fig. 1), below which the spinel coexists with Mn_2O_3. Our assumption is supported by the fact that the existence of the secondary phase Mn_2O_3 at lower temperatures was confirmed in many earlier investigations [24, 47, 48]. The second discontinuity in the slope of the TG signal in Fig. 4 takes place at 695 °C above which the mass decreases drastically. We assume that this temperature is the upper critical temperature, T_{c1} (see Eq. (1)), and indeed it corresponds well to the phase transition temperature determined in situ by means of XRD (650–700 °C, see Table 3). The third discontinuity at T_{c2} = 940 °C corresponds to the formation of $LiMnO_2$ as already reported in [24].

Between 451 and 695 °C a small weight increase is observed, which was also mentioned in other works [49]. This weight change results naturally from the oxygen exchange between the sample and the surrounding atmosphere causing a change in the oxygen nonstoichiometry, δ, of the spinel $Li_{1+x}Mn_{2-x}O_{4-\delta}$ (as already discussed in Section ''Schematic spinel stability field and experimental strategy''). In principle, the measured values of $\Delta\delta$ after a temperature change at pO_2 = const. could be used to model the defect structure of the spinel. This modeling is, however, much easier, if $\Delta\delta$ is measured after a pO_2-jump at constant temperature, as the different defects normally show power-law dependencies on pO_2 [50], with exponents that are typical of the prevailing disorder type (cation vacancy, cation interstitial or oxygen vacancy). The results of such measurements will be published in a forthcoming article [36].

Figure 5 shows a typical TG plot for a spinel with Li-deficit (n_{Li}/n_{Mn} = 0.455). The sample was heated from room temperature up to 1000 °C at 1 °C/min under pO_2 = 0.2 bar. The mass increase at temperatures below 500 °C probably refers to the formation of Mn_2O_3 (oxidation), which was not fully formed during the previous cooling process. Above 500 °C the amount of Mn_2O_3 starts to decrease (reduction) as the phase boundary of the spinel stability field is approached (see Fig. 1). Two discontinuous changes of the slope of the TG signal were observed at 614 and 868 °C, respectively. These temperatures are attributed to T_{cL} and T_{c1}, respectively where the reactions in Eqs. (2) and (1) take place. The value T_{c1} = 868 °C is in good agreement with the value determined by in situ XRD (850–900 °C, see Table 3). Both T_{cL} and T_{c1} for the lithium-deficient spinel, n_{Li}/n_{Mn} = 0.455, are much higher than those of the lithium-excess spinel, n_{Li}/n_{Mn} = 0.564. The third discontinuity at T_{c2} = 940 °C corresponds again to the formation of $LiMnO_2$. The identical values of T_{c2} for lithium-deficient and lithium excess spinels confirm that $LiMnO_2$ is essentially a line compound and is stable only above 940 °C.

To check whether the heating rate during the TG experiments has a significant influence on the critical temperatures, experiments were performed at a smaller heating rate of 0.5 °C/min. The critical

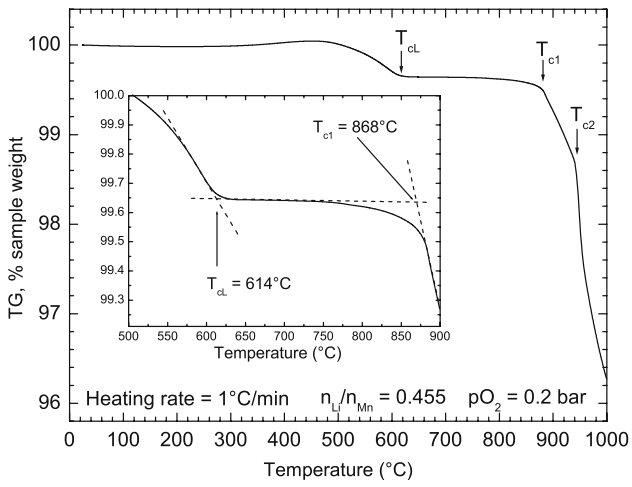

Fig. 5 Relative mass change during heating of a Li-deficient spinel (n_{Li}/n_{Mn} = 0.455) from RT to 1000 °C. The inset displays how the critical temperatures, T_{cL} and T_{c1}, were determined. At T_{c2} $LiMnO_2$ starts to form

[2] All measurements of the critical temperatures, T_{c1} and T_{cL}, contain similar errors of about ±3 °C.

temperatures obtained agree within ±2 °C with the values obtained with our standard heating rate of 1 °C/min.

Stability field of the spinel $Li_{1+x}Mn_{2-x}O_4$

All values for the critical temperatures T_{c1} and T_{cL} that were determined at $pO_2 = 0.2$ bar by TG for a series of samples with different compositions are shown in Fig. 6. The values for T_{c1} lie within the corresponding temperature intervals determined by in situ XRD (see Table 3). The single phase spinel, $Li_{1+x}Mn_{2-x}O_4$, is stable only for temperatures between the lower and upper critical temperatures, T_{cL} and T_{c1}. Both temperatures decrease with increasing lithium content, n_{Li}/n_{Mn}. Compared to the phase diagram presented by Paulsen et al. [24] (dashed lines in Fig. 6) the single phase spinel region determined in our work is broader. In addition, no discontinuities in the critical temperature curves were found between the regions of lithium excess and deficit at $n_{Li}/n_{Mn} = 0.5$ as reported by Paulsen et al. Moreover, according to our experimental results, the Li-deficient spinel region reported by Paulsen et al. is already the two-phase region where the spinel coexists with Li_2MnO_3.

Our continuous critical temperature curve, $T_{c1}(r)$, in Fig. 6 is also supported by experiments where the whole critical temperature curve is measured in a single experiment. As already discussed in Section ''Schematic spinel stability field and experimental strategy'', the whole curve $T_{c1}(r)$ can be obtained if one reference point, $T_{c1}(r_1)$, on the curve is known. Heating the single phase spinel slowly from $T_{c1}(r_1)$ to T_2 (see Eq. (1) and Fig. 1), the amounts of spinel, $a_2(T)$, and of Li_2MnO_4, $b_2(T)$, as well as the cation composition, $x_2(T)$, can be determined for each temperature by measuring the mass change, $c_2(T)$, during heating and using the three mass balances for Li, Mn and O in Eq. (1). The results are shown as broken lines in Fig. 7 for four different reference points. None of the four curves shows a discontinuity at $n_{Li}/n_{Mn} = 0.5$ as reported in [24], and all curves coincide well with the points determined individually from the TG measurements of samples of different cation compositions.

The upper and lower critical temperatures, T_{c1} and T_{cL}, were also investigated by TG under different oxygen partial pressures, pO_2, for samples with different cation compositions, n_{Li}/n_{Mn}. The results in Fig. 8 show that that both T_{c1} and T_{cL} are not only dependent on n_{Li}/n_{Mn} but also linear functions of $\log(pO_2)$. Both critical temperatures increase with increasing pO_2. It indicates that the spinel decomposes to spinel and Mn_2O_3 during oxidation and to spinel and Li_2MnO_3 during reduction, respectively.

Our experimental findings for the dependence of the lower and upper critical temperatures of the stability field of Li–Mn–O spinel on the cation composition, n_{Li}/n_{Mn}, and the oxygen partial pressure, pO_2, are summarized in the three-dimensional diagram in Fig. 9. The two areas in the figure represent the boundaries of the spinel $Li_{1+x}Mn_{2-x}O_4$.

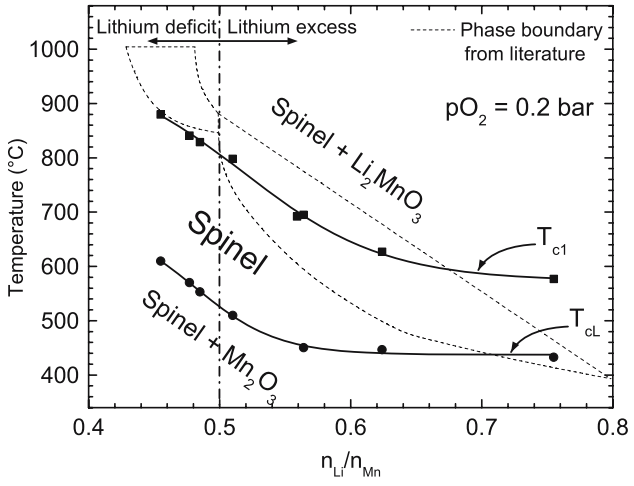

Fig. 6 Dependence of upper and lower critical temperatures, T_{c1} and T_{cL}, on cation composition, n_{Li}/n_{Mn} (symbols; the solid lines are only a guide to the eye). For comparison the phase boundaries according to Paulsen et al. [24] are shown (dashed lines)

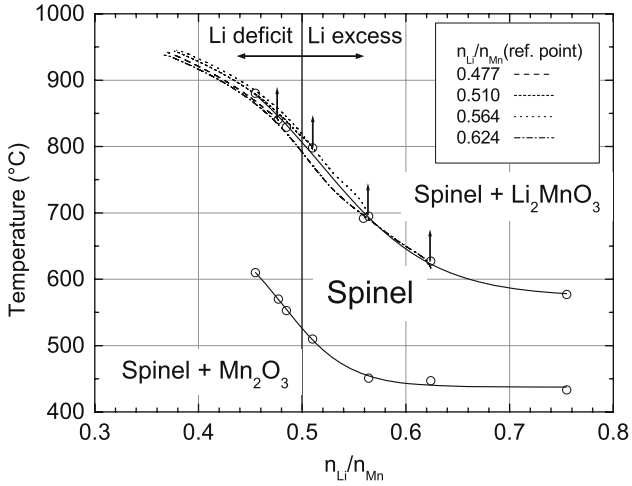

Fig. 7 Lower and upper critical temperatures, T_{cL} and T_{c1}, of the spinel stability field as determined by means of TG on samples of different compositions (open circles, the solid lines are only guide to the eye) and upper critical temperature curves, $T_{c1}(r)$ (broken lines), as determined during continuous heating of a single spinel sample starting at the reference point marked by an arrow

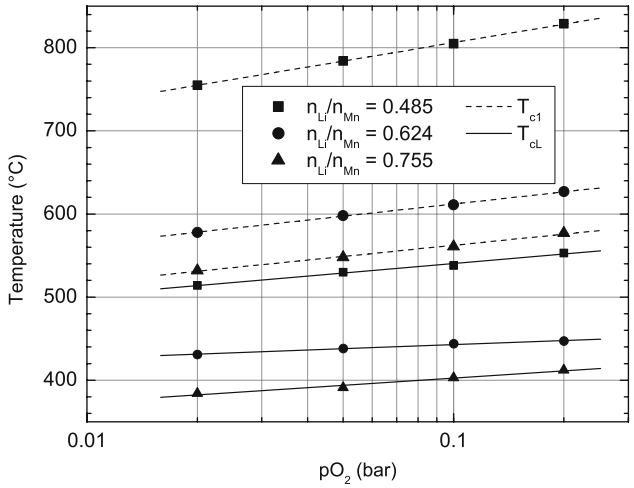

Fig. 8 Dependence of critical temperatures, T_{cL} and T_{c1}, on oxygen partial pressure, pO_2, for different cation compositions, n_{Li}/n_{Mn}

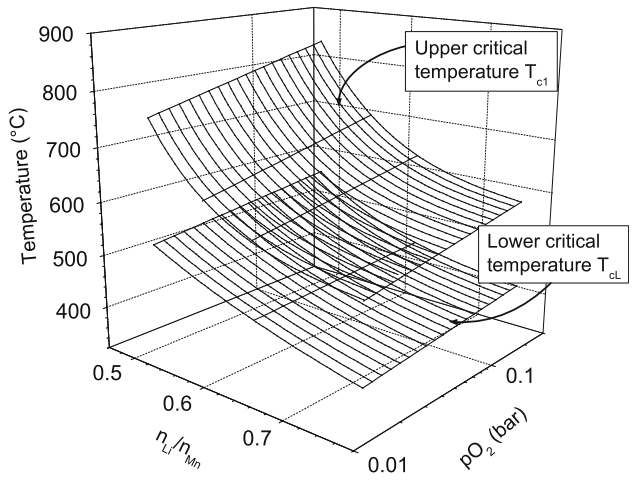

Fig. 9 Three-dimensional stability field of Li–Mn–O spinel

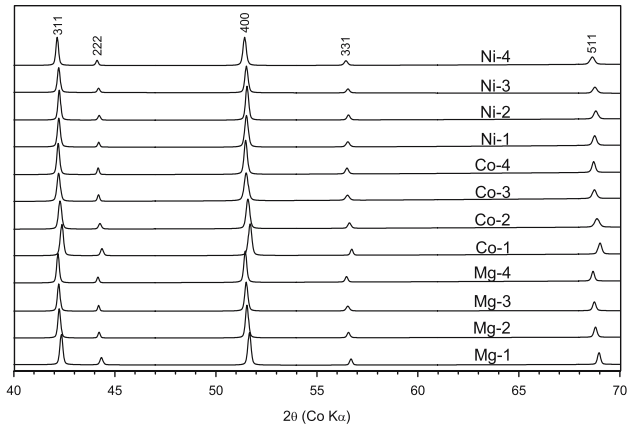

Fig. 10 XRD patterns of doped Li–Mn–O samples (see Table 2) measured at room temperature. All peaks are spinel peaks

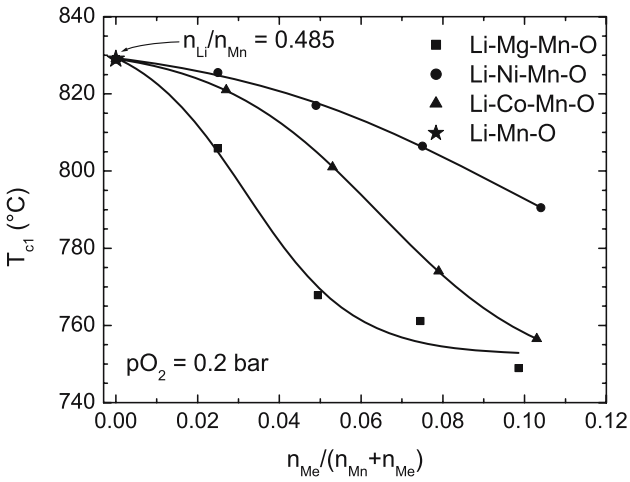

Fig. 11 Dependence of upper critical temperature, T_{c1}, on dopant fraction

Stability of doped spinels $Li_{1+x}(Mn,Me)_{2-x}O_4$

X-ray diffraction at room temperature (Co Kα, λ = 178.9007 pm) shows that all as prepared, doped Li–Mn–Me–O (Me = Mg, Ni, Co) spinels (see Table 2) are single phase spinels (see Fig. 10).

In order to investigate the thermal stability of the doped spinels, TG experiments were performed as for the undoped samples, i.e. by heating with 1 °C/min to 1000 °C in air. It was found that all doped samples exhibit similar TG characteristics as the undoped samples. However, only the upper critical temperature could be determined accurately (see Fig. 11). For a determination of the lower critical temperature the observed mass changes were too small, probably caused by the small total sample masses in these experiments. Further TG measurements are required using bigger sample masses.

For all three dopants, Mg, Ni and Co, the upper critical temperatures, T_{c1}, of the doped spinels decrease with increasing dopant fraction, where the Mg-doped spinel shows the worst stability. Apparently, doping with Mg, Ni or Co has the same effect on the upper critical temperature, T_{c1}, as ''doping'' with excess lithium, i.e. T_{c1} decreases and the spinel is less stable at elevated temperatures. To our knowledge, this is the first quantitative measurement to investigate the influence of dopants on T_{c1}.

Summary

The thermal stability of lithium–manganese spinels, $Li_{1+x}Mn_{2-x}O_4$, was investigated by in situ X-ray

diffraction (XRD) and thermogravimetry (TG). In a temperature versus cation composition phase diagram, the spinel stability field is limited by two temperature curves, the upper critical temperature, T_{c1}, above which the spinel coexists with monoclinic Li_2MnO_3, and the lower critical temperature curve, T_{cL}, below which the spinel coexists with Mn_2O_3. While in situ XRD only rendered possible a rough determination of the upper critical temperature curve, T_{c1}, an accurate determination of both the lower and upper critical temperature curves was possible by TG. Both T_{cL} and T_{c1} are continuous functions of the cation composition, n_{Li}/n_{Mn}, i.e. no discontinuities are found in the critical temperature lines between the Li-excess and Li-deficit regions (as reported in earlier phase diagrams). Lithium deficient spinel is stable at higher temperatures than lithium excess spinel. Both T_{cL} and T_{c1} are functions of oxygen partial pressure, pO_2, and increase linearly with increasing $\log(pO_2)$. Leaving the stability field of the spinel by means of isothermal oxidation results in the appearance of Mn_2O_3, while reduction yields Li_2MnO_3 as second phase. For doped Li–Me–Mn–O (Me = Mg, Ni, Co) spinels the upper critical temperature, T_{c1}, is dependent on the type of dopant, $T_{c1}(Mg) < T_{c1}(Co) < T_{c1}(Ni)$, but decreases for all of them with increasing dopant fraction.

The results on the stability field of the Li–Mn-spinel form the basis for our investigations on the defect structure of the spinel which will be published in part II of this article [36]. In these experiments changes of the oxygen nonstoichiometry, $\Delta\delta$, of the spinel $Li_{1+x}Mn_{2-x}O_{4-\delta}$ are determined after isothermal pO_2-jumps. Modeling of the experimental results yields insight into the high temperature defect structure of Li–Mn-spinel and allows an identification of the majority defects that are important for mass and charge transport phenomena in the spinel.

Acknowledgement C. Luo thanks the Friedrich-Ebert-Stiftung for a scholarship. We thank H. Lippert at Forschungszentrum Jülich for performing the ICP-OES analysis. Support by the Fonds der chemischen Industrie (FCI) is gratefully acknowledged.

References

1. Tarascon JM, Armand M (2001) Nature 414:359
2. Vincent CA (2000) Solid State Ionics 134:159
3. Thackeray MM (1999) J Am Ceram Soc 82:3347
4. Thackeray MM, David WIF, Bruce PG, Goodenough JB (1983) Mater Res Bull 18:461
5. Sickafus KE, Wills JM, Grimes NW (1999) J Am Ceram Soc 82:3279
6. Akimoto J, Takahashi Y, Gotoh Y, Mizuta S (2001) J Cryst Growth 229:405
7. Yamada A, Tanaka M (1995) Mater Res Bull 30:715
8. Yamada A, Tanaka M, Tanaka K, Sekai K (1999) J Power Sources 81–82:73
9. Amine K, Tukamoto H, Yasuda H, Fujita Y (1997) J Power Sources 68:604
10. Myung ST, Komaba S, Kunagai N (2001) J Electrochem Soc 148:A482
11. Wamg GX, Bradhurst DH, Liu HK, Dou SX (1999) Solid State Ionics 120:95
12. Hong YS, Han CH, Kim K, Kwon CW, Campet G, Choy JH (2001) Solid State Ionics 139:75
13. Bellitto C, Dimarco MG, Branford WR, Green MA, Neumann DA (2001) Solid State Ionics 140:77
14. Wu C, Wang Z, Wu F, Chen L, Huang X (2001) Solid State Ionics 144:277
15. Shen CH, Liu RS, Gundakaram R, Chen JM, Huang SM, Chen JS, Wang CM (2001) J Power Sources 102:21
16. Choi HJ, Lee KM, Lee JG (2001) J Power Sources 103:154
17. Bonino F, Panero S, Satolli D, Scrosati B (2001) J Power Sources 97–98:389
18. Li G, Iijima Y, Kudo Y, Azuma H (2002) Solid State Ionics 146:55
19. Huang K, Peng B, Chen Z, Huang P (2000) Solar Energy Mater Sol Cells 62:177
20. Kilroy WP, Ferrando WA, Dallek S (2001) J Power Sources 97–98:336
21. Tabuchi M, Masquelier C, Kobayashi H, Kanno R, Kobayashi Y, Akai T, Maki Y, Kageyama H, Nakamura O (1997) J Power Sources 68:623
22. Molenda J, Kucza W (1999) Solid State Ionics 117:41
23. Takada T, Hayakawa H, Akiba E, Izumi F, Chakoumakos BC (1997) J Power Sources 68:613
24. Paulsen JM, Dahn JR (1999) Chem Mater 11:3065
25. Kelder EM, Jak MJG, Schoonman J, Hardgrave MT, De Andersen SY (1997) J Power Sources 68:590
26. Thackeray MM, Mansuetto MF, Dees DW, Vissers DR (1996) Mater Res Bull 31:133
27. Choi S, Manthiram A (2000) J Electrochem. Soc 147:1623
28. Thackeray MM, Mansuetto MF, Bates JB (1997) J Power Sources 68:153
29. Liu Y, Fujiwara T, Yukawa H, Morinaga M (1999) Solid State Ionics 126:209
30. Gao Y, Dahn JR (1996) J Electrochem Soc 143:1783
31. Gao Y, Dahn JR (1995) Appl Phys Lett 66:2487
32. Gao Y, Dahn JR (1996) J Electrochem Soc 143:100
33. Yamada A, Miura K, Hinokuma K, Tanaka M (1995) J Electrochem Soc 142:2149
34. Tarascon JM, McKinnon WR, Coowar F, Bowmer TN, Amatucci G, Guyomard D (1994) J Electrochem Soc 141:1421
35. Luo C, Martin M (2003) In: Zaghib K, Julien CM, Prakash J (eds) Proceedings of the electrochemical society 203rd meeting, Paris. PV 2003–20, p 281
36. Luo C, Martin M to be published
37. Pechini MP (1963) US-Patent 3 330 697
38. Mascarenhas YP, Cavalheira AA, Zaghete MA, Paiva-Santos CO, Silva Giotto MT, Cilense M, Varela JA (2001) Key Eng Mater 189–191:27
39. Liu W, Farrington GC, Chaput F, Dunn B (1996) J Electrochem Soc 143:879
40. Buhrmester T, Martin M (2000) Solid State Ionics 135:267
41. Han YS, Kim HG (2000) J Power Sources 88:161
42. Gummow RJ, de Kock A, Thackeray MM (1994) Solid State Ionics 69:59
43. Chung HT, Myung ST, Cho TH, Son JT (2001) J Power Sources 97–98:454
44. Lee YJ, Grey CP (2002) J Electrochem Soc 149:A103

45. Xia Y, Sakai T, Fujieda T, Yang XQ, Sun X, Ma ZF, McBreen J, Yoshio M (2001) J Electrochem Soc 148:A723
46. Björk H, Dabkowska H, Greedan JE, Gustafsson T, Thomasa JO (2001) Acta Cryst Sect C: Cryst Struct Commun C57:331
47. Hwang BJ, Santhanam R, Liu DG (2001) J Power Sources 97–98:443
48. Wickham DG, Croft WJ (1958) J Phys Chem Solids 7:351
49. Dziembaj R, Molenda M, Majda D, Walas S (2003) Solid State Ionics 157:81
50. Martin M (2005) In: Heitjans P, Kärger J (eds) Diffusion in condensed matter, methods, materials, models. Springer, p 209